Low temperature dry methane reforming over Ce, Zr and CeZr promoted Ni–Mg–Al hydrotalcite-derived catalysts

Radoslaw Dębek, Maria Elena Galvez, Franck Launay, Monika Motak, Teresa Grzybek, Patrick da Costa

Low temperature dry methane reforming over Ce, Zr and CeZr promoted Ni-Mg-Al hydrotalcite-derived catalysts

Radosław Dębek[a,b,c], Maria Elena Galvez[b,c], Franck Launay[d,e], Monika Motak[a], Teresa Grzybek[a], Patrick Da Costa[b,c*]

[a] AGH University of Science and Technology, Faculty of Energy and Fuels, Al. A. Mickiewicza 30, 30-059 Kraków, Poland

[b] UPMC, Univ Paris 06, Sorbonne Universités, Institut Jean Le Rond d'Alembert, 2 Place de la Gare de Ceinture, 78210 Saint Cyr l'Ecole, France.

[c] CNRS, UMR 7190, Institut Jean Le Rond d'Alembert, 2 place de la Gare de Ceinture, 78210 Saint Cyr l'Ecole, France.

[d] UPMC Univ Paris 06, Sorbonne Université, Laboratoire de Réactivité de Surface, 4 Place Jussieu, 75005, Paris, France

[e] CNRS, UMR 7197, Laboratoire de Réactivité de Surface, 4 Place Jussieu, 75005, Paris, France

Abstract

Hydrotalcite derived catalysts promoted with Ce, Zr and CeZr showed considerable activity in dry methane reforming (DMR) at low temperatures (550°C). Direct methane decomposition resulting in the extensive formation of fishbone-type carbon nanofibers was substantially inhibited in the presence of Zr. Physicochemical characterization by means of N_2 adsorption, XRD, TPR and CO_2-TPD evidenced narrower porosity and higher surface areas for the Zr-containing catalysts, together with the presence of smaller Ni particles (around 4 nm) and CO_2 preferential adsorption in weak basic sites. Such small Ni particles are inactive towards the direct methane decomposition reaction. The ability of the Zr-containing catalysts to adsorb CO_2 on weak basic sites results in the formation of active carbonate species that are able to react with methane through the DMR route. The reverse Boudouard reaction occurs simultaneously to a certain extent in the presence of Zr-promoted catalyst, since carbon nanotube formations were visible on the catalyst surface upon its utilization.

Keywords: Hydrotalcite materials, nickel catalysts, methane dry reforming, syngas, hydrogen.

[*] Corresponding author: patric.da_costa@upmc.fr, tel.: +33 1 30 85 48 62

1. Introduction

Dry methane reforming (DMR) has attracted considerable attention in the last decades as a perspective method for CO_2 valorization, yielding an equimolar mixture of H_2 and CO. Such a syngas can be directly used for liquid fuel synthesis through the Fischer-Tropsch process, or for the production of valuable oxygenated compounds [1, 2]. However, the DMR process presents still important drawbacks towards its practical application, mainly related to the simultaneous occurrence of carbon-forming reactions, such as direct methane decomposition, and, to a lesser extent, the Boudouard reaction [3-5].

Nickel-containing catalysts have been recently presented as a promising alternative to noble metal based ones [5-11]. Among these materials, the catalysts obtained through the thermal decomposition of layered double hydroxides, i.e. hydrotalcites, have been recently reported to show interesting catalytic performance over long-run catalytic tests [10-16] and at relatively low temperatures [17, 18]. Calcination results in an homogeneous mixture of finely dispersed M^{II} and M^{III} oxides, having high thermal stability among other very interesting physico-chemical features. Moreover, varying the molar ratio allows the tailoring of these properties, i.e. their intrinsic basicity and redox properties. Gonzalez et al. [12] studied Ni-Mg-Al hydrotalcite derived oxides obtained by sol-gel method with different nickel content – 4, 15 and 19 wt.%. The prepared catalysts showed high activity and stability at 800°C. Perez-Lopez et al. [13] synthesized Ni-Mg-Al hydrotalcites with different Ni/Mg and M^{2+}/M^{3+} molar ratios by a co-precipitation method at constant pH. The composition of the catalyst precursor had a large influence on catalyst performance, i.e. catalytic activity was mainly affected by the M^{2+}/M^{3+} molar ratio. More recently, several hydrotalcite-like materials were prepared and tested in DMR, using different Ni/Mg molar ratios for a fixed value of M^{2+}/M^{3+} = 3, typical of the naturally occurring Mg-Al hydrotalcite [17, 18].

Catalytic activity and thermal stability of Ni-based catalysts can be improved by means of using promoters such as CeO_2 and/or ZrO_2. The addition of Ce-species into the catalytic hydrotalcite-based structure was found to promote the reducibility of the nickel species and resulted in the introduction of new strong (low coordinated) oxygen species and intermediate (Lewis acid-base pairs) strength basic sites, which increased the CO_2 adsorption capacity of the catalysts [18]. Moreover, ZrO_2 may increase the content in oxygen vacancies on the catalyst surface, which are of key importance for the dissociative adsorption of CO_2 [19, 20].

In the present paper Ni-Mg-Al hydrotalcite-derived catalysts were prepared, promoted either with Ce, Zr and CeZr. In all cases, the Ni/Mg and M^{2+}/M^{3+} molar ratios were kept respectively around 0.3 and 3, corresponding to a Ni-content of approximately 20 wt.%. Their activity and selectivity towards DMR was tested at low temperatures, i.e. 550°C, with special attention on the carbon formation reactions leading to catalyst deactivation. The textural, structural and chemical features of the promoted catalysts were carefully studied in order to identify the key mechanisms leading to the suppresion of extensive carbon deposition.

2. Experimental

2.1. Catalysts preparation

The hydrotalcite catalyst precursors were obtained by co-precipitation from an aqueous solution of Mg, Ni and Al nitrates (POCH), using a 0.05 M sodium carbonate (Acros Organics) solution and 1 M NaOH (POCH), corresponding to a nominal Ni content of 25 wt.%. The nitrate solution with M^{2+}/M^{3+} molar ratio equal to 3 and 1 M NaOH were added drop-wise into the sodium carbonate solution at 60°C and at fixed pH of 10 ± 0.2. The obtained suspension was kept under vigorous stirring for 1 h, then filtered and dried overnight at 80°C. In case of zirconia promoted samples, the zirconium species were introduced into hydrotalcite structure at the co-precipitation stage. The zirconium oxynitrate was used as Zr^{4+} precursor. The molar ratio of Al^{3+}/Zr^{4+} was equal to 9/1. In order to introduce Ce-species into the hydrotalcite precursors, these materials were kept in contact with a 3% wt. aqueous solution of [Ce(EDTA)]−complexes for 24 h at room temperature. The hydrotalcite materials were subsequently calcined at 550°C for 4 h. Four different catalysts were prepared: HT-25Ni, prepared without either Ce or Zr, HTNi-Ce, promoted with Ce, HTNi-Zr, promoted with Zr, and HTNi-CeZr, promoted with both Ce and Zr.

2.2. Catalysts characterization

The elemental analysis of the hydrotalcite-derived catalysts was performed by means of XRF using an energy dispersive XEPOS spectrometer (Spectro Ametek). The sample was analyzed in its powder form. Quantitative data were determined using the MicroPowder method. XRD patterns were acquired in an Empyrean diffractometer from PANalytical, equipped with CuK_α anode (λ = 0.154059 nm). Temperature programmed reduction (H_2-TPR) profiles were acquired in a BELCAT-M device from BEL Japan, equipped with a thermal conductivity detector (TCD). The materials (50 mg) were firstly outgassed at 100°C

for 2 h and then reduced using 5%H_2/Ar at a heating rate of 7.5°C/min. The basicity of these catalysts was evaluated by means of CO_2-temperature programmed desorption in the BELCAT-M apparatus. 60 mg of material were first degassed for 2 h at 500°C, then cooled down to 80°C. A mixture of 10%CO_2/He was then fed for 1 h during the adsorption step. A flow of He was subsequently fed for 15 minutes in order to desorb the physically adsorbed CO_2. The material was then heated up under He at 10°C/min, while the evolution of CO_2 was measured with the aid of the TC detector. Textural parameters of the different materials were calculated from their corresponding N_2 adsorption isotherms obtained at −196°C in a Belsorp Mini II apparatus from BEL Japan. Thermogravimetric measurements were carried out with a SDT Q600 apparatus (TA Instruments), under air flow (100 mL/min) heating from ambient temperature to 900°C at a rate of 10 °C/min.

2.3. Dry methane reforming (DMR) experiments

The activity and selectivity of the different HT-derived catalysts was assayed in a tubular quartz reactor of 1.2 cm diameter, heated by a cylindrical resistive electric furnace. Temperature was measured inside the catalytic bed, with the aid of a quartz-shielded K-type thermocouple. A total flow of reactant gas mixture of 100 mL/min consisting of CH_4/CO_2/Ar = 1/1/8 was fed using several mass flow controllers (BROOKS 5850E). Under such conditions, the gas hourly space velocity (GHSV) corresponded to 20,000 h^{-1}, i.e. approximately 200 mg of catalyst, 0.2 mm particle size, non inert-diluted. The catalysts were reduced in situ at 900°C during 1 h, using a 3%H_2/Ar mixture. After reduction, the catalysts were cooled down to 550°C and the reactant gas mixture was supplied to the reactor. The analysis of the products was carried out on-line in a Varian GC490 micro chromatograph equipped with a thermal conductivity detector (TCD).

3. Results and discussion

3.1. Activity and selectivity in DMR

Figure 1 a, b and c show the methane and CO_2 conversions, together with the H_2/CO ratio, measured during the DMR experiments at 550°C, in the presence of the different HT-derived catalysts. Even at this low reaction temperature, the HT-derived catalysts are notably active towards methane dry reforming. Upon 5 h time-on-stream, the catalysts present no evidences of deactivation.

The Ce-containing catalyst, HTNi-Ce, behaves similarly to the catalyst containing only Ni, HT-25Ni. Both methane and CO_2 conversion reach comparable values, both around 40%, with methane conversion being slightly higher in the case of HT-25Ni. The lower methane conversion measured for HTNi-Ce, together with the higher values of H_2/CO ratio, close to the desired value of 1, point to a slightly positive effect of Ce, which may avoid to a certain point the occurrence of the simultaneous direct methane decomposition reaction [18]. The promoting effect of Ce is widely known and has been ascribed to its large oxygen storage capacity, which might be favoring the oxidation of the carbon deposits formed upon direct methane decomposition [18, 19]. Note here that the thermodynamic analysis of the DMR reaction set (performed with the aid HSC 5.0 Outokumpu software) predicts a CO_2 conversion around 43%, and around 83% for methane, resulting in high H_2/CO ratios around 4.

When Zr is present in the catalyst formulation, both methane and CO_2 conversions are considerably lower, i.e. 25% CH_4 conversion and 30% CO_2 conversion after 300 min time-on-stream for HTNi-CeZr. In fact, the values of CO_2 conversion are all the time relatively higher than the values of methane conversion for these Zr-containing catalysts, opposite to the thermodynamically forecasted trends. This is directly reflected in the H_2/CO ratios measured during the DMR experiments, which are considerably lower than for HT-25Ni and HTNi-Ce, especially for the catalyst that does not contain Ce, i.e. HTNi-Zr. Zirconia thus modifies the selectivity of the catalysts resulting in an excess of CO in the syngas mixture. Direct methane decomposition is substantially inhibited, as well as the water gas shift reaction, since no excess of H_2 is detected. Other reactions, such as either the direct or the reverse Boudouard reaction, $2CO = CO_2 + C$, might be significantly favored [20, 21].

3.2. Influence of Ce, Zr and CeZr on catalyst stability: Carbon formation

From the activity plots shown in Figure 1, it becomes clear that competitive reactions, such as methane direct decomposition and the Boudouard reaction may be happening to a certain extent in the presence of the different HT-derived catalysts. The study and quantification of the carbon deposits formed can be very helpful in determining the role of the presence of Ce and Zr in the formulation of these catalysts. Transition electron microscopy images are shown in Figure 2, for the HT-derived catalysts after 300 min of DMR reaction at 500°C. The spent HT-25Ni and HTNi-Ce catalysts contain plenty of carbon deposits. The original particles of both catalysts appear almost completely covered by these carbon formations. Ni particles are still visible, most of them detached from the HT-derived mixed

oxide structure and at the end of well-developed fishbone carbon nanofibers. These fibers contain several graphite planes, with thicknesses varying from 5 to 20 nm. In the case of the Ce containing catalyst, the fiber structures contain more defects and appear frequently broken or damaged, but still covering an important part of the active surface.

Such fiber structures are completely absent in the case of the spent catalyst containing Zr, HTNi-Zr and HTNi-CeZr. Carbon formations resembling multi and even single wall carbon nanotubes are present on the surface and growing out of the catalyst surface. These carbon filaments are composed of only 1 to 4 graphite planar layers, sometimes forming bamboo-like structures, and all the time much thinner than the fishbone fibers observed for HT-25Ni and HTNi-Ce. For the Ce-containing catalyst, HTNi-CeZr, some fishbone structures can be found, but their presence is minimal in comparison to HTNi-Ce. The presence of Zr has therefore a definitive influence on the type of carbon deposits formed. According to the TEM images acquired for the spent HT-derived catalysts, it seems that Zr substantially inhibits the formation of carbon fibers through the direct methane decomposition. ~~reaction and might promote other routes for carbon formation, i.e. the Boudouard reaction~~.

The thermogravimetric oxidation of the carbon deposits formed on the surface of the catalysts upon reaction yields further information on their amount and thermal stability. Figure 3 contains the thermogravimetric curves, i.e. the derivative of the weight-loss registered as a function of temperature, for the different HT-derived spent catalysts. It can be clearly observed that, in the presence of the catalysts HT-25Ni and HTNi-Ce, greater amounts of carbon deposits are formed upon 300 min DMR reaction at 550°C, as indicated by each corresponding peak in the DTGA signal appearing at temperatures between 450 and 650°C. These carbon deposits (the fishbone fibers observed in Figure 2 a and b) are oxidized at lower temperatures in the presence of Ce, i.e. the DTGA peak appears at lower temperatures, the difference between the two maxima being approximately 25°C.

The thermogravimetric curves are completely different for the Zr-containing catalysts. A wide DTGA peak starting at temperatures around 300°C and extending up to maximally 525°C appears for both HTNi-Zr and HTNi-CeZr. Since the area of these peaks is much smaller, one can definitively conclude from this plots that carbon formation upon DMR reaction is minimal, in any case substantially reduced, when Zr is present in the catalyst formulation vis-à-vis the other catalysts in this series that do not contain Zr. In agreement with the TEM observation of the spent catalysts, Zr seems to be able to modify the selectivity of the catalyst, activating the DMR route and to some extent the Boudouard reaction but

almost completely inhibiting the direct methane decomposition reaction. The use of Zr as a promoter in these HT-derived catalysts seems to be therefore a warranty for high catalyst stability.

3.3. Physicochemical features of the Ce, Zr and CeZr doped HT-derived catalysts: the role of Zr in the DMR reaction.

The textural, structural and chemical properties of the different HT-derived materials promoted with either Ce, Zr or CeZr were determined, in order to clarify their influence on the activity and selectivity of these catalysts, and to elucidate the role of the different promoting species. Table 1 shows the composition of the different catalysts, as determined by XRF. A Ni content between 17.3 and 19.6 wt.% was measured for all the catalysts. Ni/Mg ratios are all the time close to 0.3, corresponding to a ratio M^{2+}/M^{3+} around 3, the typical value in naturally existing hydrotalcites. Let us note here that the values of this molar ratio presented in Table 1 slightly differ from the nominal value of 3, i.e. 3.51 for HTNi-CeZr. This may come from the co-precipitation procedure leading to the raw hydrotalcite structure, and to the possible influence of the presence of Zr cations on pH modification resulting in such slightly higher M^{2+}/M^{3+} ratios. Ce content in both HTNi-Ce and HTNi-CeZr was found to be 3.7 and 4.7 wt.%, respectively. Zr contents of 2.5 to 2.7 wt.% was measured for both HTNi-Zr and HTNi-CeZr.

The values of surface area, S_{BET}, total pore volume, V_p, and mean pore size, derived from the N_2 adsorption isotherms acquired for the different HT-derived catalysts are presented as well in Table 1. The catalyst HT-25Ni shows values of surface area, total pore volume and mean pore size typical of mesoporous hydrotacite-derived Mg-Al-Ni mixed oxides [22, 23]. Zr-doping results in HT-derived mixed oxides of higher surface area, i.e. S_{BET} increases from 115 to 229 m^2/g, due to the creation of smaller pores of mean diameter around 2 nm. The simultaneous presence of Ce results in a material, HTNi-CeZr, having still higher surface area, S_{BET} = 158 m^2/g, and intermediate pore sizes, i.e. 4.7 nm. This increase in surface area and the favored presence of narrower pores should explain a higher resistance towards deactivation due to impeded growth of carbon fibers, but does not provide itself an explanation to the lower activity, or to the substantially hindered direct methane decomposition reaction in the presence of the Zr-containing catalysts.

The XRD patterns acquired for the fresh hydrotalcite materials and the calcined HT-derived catalysts are shown in Figure 4 a and b. Before calcination, Figure 4 a, all the materials show the typical layered structure of hydrotalcite [22, 23]. The absence of any other

additional crystalline phase in the diffractograms points to successful incorporation of nickel cations into the brucite-like layers. The XRD patterns for the calcined HT-derived catalysts, Figure 1 b, evidence two main reflections at 43.5 and 63°, which can be assigned to the periclase-like structure of mixed Ni-Mg oxides generated upon the thermal decomposition of hydrotalcite materials [23].

The intensity of the (111) reflection, appearing around 35°, decreases in the presence of Zr. It becomes wider, and seems to be directly related to the size of Ni-crystallites, being thus smaller for the Zr-containing catalysts. TEM observation, together with the histograms plotted for the micrographs corresponding to each HT-derived catalyst, further confirm this fact. Mean particle size from these histograms was found to decrease from around 10-12 nm in HTNi-25 and HTNi-Ce to 3-5 nm in HTNi-Zr and HTNi-CeZr. There is thus a considerable effect of the presence of Zr in the Ni particle size that can explain, up to a certain point, the differences in the selectivity observed for the HT-derived catalysts towards the different reactions involved. It has been previously reported [5] that bigger Ni particles enhance the direct methane decomposition reaction, favoring its deactivation through the extensive formation of carbon deposits. This reaction should be thus substantially inhibited when smaller Ni particles are present, i.e. as it was observed for the Zr-containing catalysts. Moreover, CO_2 adsorption is enhanced on small metal particles [21], what will favor the reverse Boudouard reaction, resulting in increased CO formation (see the low H_2/CO ratios registered for the Zr-containing catalysts). Note that the presence of a separate CeO_2 phase in Ce-promoted catalyst, fluorite-type structure, has been previously reported [18].

Temperature programmed reduction yields further information on the reducibility and dispersion of the different active species contained in this series of HT-derived catalysts. TPR curves are shown in Figure 5 a. As previously observed, the presence of Ce favors the reducibility of Ni species, as pointed out by the shift of the main peak appearing on the TPR profile to lower reaction temperatures. The peak for HTNi-Zr appears centered at relatively higher temperatures, i.e. 25°C higher than for HT-25Ni, corresponding to the more difficult reduction of smaller Ni particles, in complete agreement with TEM observation and XRD.

The temperature programmed desorption curves acquired upon CO_2 adsorption for the Ce, Zr and CeZr containing catalysts after reduction at 900°C for 2 h are shown in Figure 5 b. CO_2 desorption at different temperatures allows the determination of the basicity of each catalyst, which is substantially modified by the presence of the Ce and Zr promoters. Hydrotalcite-derived materials exhibit three CO_2 desorption peaks in temperature range 100–

500°C [24-26]. The first desorption peak observed at 100-150°C is attributed to the desorption of CO_2 from weak Brønsted OH groups, the peak observed at ca.190°C can be assigned to the formation of bidentate carbonates formed on metal-oxygen pairs, and finally the CO_2 adsorbed on strong basic sites is desorbed at temperatures higher than 280°C [24, 25]. The presence of Zr substantially hinders the adsorption of CO_2 in these last strong basic sites, normally CO_2 bonded on low-coordination oxygen anions, since no peak is detected in the TPD profile for HTNi-Zr. On the contrary, the presence of Ce seems to favor this kind of strong basicity. The CO_2 adsorbed on strong basic sites reacts more difficultly with methane and direct methane decomposition is therefore enhanced, above all in the presence of relatively big Ni particles. Though it is still to early to state anything about the reaction mechanism in the presence of Zr, it is clear that its presence affects the CO_2-adsorption pattern that in turn can modify the reaction pathway. Further tests and characterization need to be performed in order to clarify this fact, maybe also through the evaluation of the influence of the molar Ce/Zr ration on the catalytic behavior.

4. Conclusions

Ni-Mg-Al hydrotalcite-derived materials were synthesized in the presence of either Ce, Zr or CeZr, and used as catalysts for syngas production through dry methane reforming (DMR) at low temperatures. The presence of Zr was found to strongly determine both the activity and the selectivity of these catalysts. Zr considerably inhibited the direct methane decomposition reaction, favoring the interaction of methane with CO_2 (DMR reaction) together with other important parallel reactions such as the reverse Boudouard reaction. Though lower conversions of both methane and CO_2 were measured, almost no carbon was deposited on the catalyst surface upon 5 h of DMR reaction at 550°C. Carbon nanotubes were formed instead of the typical fishbone fibers formed upon direct methane decomposition on Ni-catalysts.

The physicochemical characterization of the catalysts evidenced the formation of narrower porosity, resulting in higher surface areas, for the Zr-containing catalysts. XRD together with TEM observation of the catalysts pointed to the presence of smaller particles, around 4 nm, in these catalysts, in comparison to the almost 12 nm measured for the catalysts prepared in the absence of Zr. Smaller Ni-particles are no longer active towards direct methane decomposition and are thought to favor other side reactions such as the reverse Boudouard reaction. Moreover, the presence of Zr was found to promote the adsorption of CO_2 on weak basic sites, resulting in favored interaction of the adsorbed bidentate carbonates with methane.

Acknowledgements

R. Debek acknowledges the International Group of Research (GDRI) “Catalysis for polluting emissions after treatment and production of renewable energies” and the French Embassy in Poland for the financial support. The present work was also founded within NCiBR strategic research project ‘Technologies supporting development of safe nuclear energy’, research task no. 1 ‘Development of high temperature reactors for industrial applications’, agreement no. SP/J/1/166183/12, step task no. 15 ‘Preparation and physicochemical characterization of catalysts for dry reforming of methane’. We kindly thank Dr. P. Beaunier at the UPMC for her guidance through the acquisition of TEM images.

References

[1] A.S. Al-Fatesh, M.A. Naeem, A.H. Fakeeha, A.E. Abasaeed, CO_2 Reforming of Methane to Produce Syngas over gamma-Al_2O_3-Supported Ni-Sr Catalysts, Bull. Chem. Soc. Jpn., 86 (2013) 742-748.

[2] M.C.J. Bradford, M.A. Vannice, Catalytic reforming of methane with carbon dioxide over nickel catalysts. 1. Catalyst characterization and activity, Appl. Catal. A: Gen., 142 (1996) 73-96.

[3] M.M. Barroso-Quiroga, A.E. Castro-Luna, Catalytic activity and effect of modifiers on Ni-based catalysts for the dry reforming of methane, Int. J. Hydrogen Energ., 35 (2010) 6052-6056.

[4] M.C.J. Bradford, M.A. Vannice, Catalytic reforming of methane with carbon dioxide over nickel catalysts. 2. Reaction, Appl. Catal. A: Gen., 142 (1996) 97-122.

[5] Y.H. Hu, E. Ruckenstein, Catalytic Conversion of Methane to Synthesis Gas by Partial Oxidation and CO_2 Reforming. In: Adv. Catal. 48 (2004) 297-345

[6] A. Albarazi, P. Beaunier, P. Da Costa, Hydrogen and syngas production by methane dry reforming on SBA-15 supported nickel catalysts: On the effect of promotion by $Ce_{0.75}Zr_{0.25}O_2$ mixed oxide, Int. J. Hydrogen Energ., 38 (2013) 127-139.

[7] Z. Alipour, M. Rezaei, F. Meshkani, Effects of support modifiers on the catalytic performance of Ni/Al_2O_3 catalyst in CO_2 reforming of methane, Fuel, 129 (2014) 197-203.

[8] F. Meshkani, M. Rezaei, Nanocrystalline MgO supported nickel-based bimetallic catalysts for carbon dioxide reforming of methane, Int. J. Hydrogen Energ., 35 (2010) 10295-10301.

[9] W. Nimwattanakul, A. Luengnaruemitchai, S. Jitkarnka, Potential of Ni supported on clinoptilolite catalysts for carbon dioxide reforming of methane, Int. J. Hydrogen Energ., 31 (2006) 93-100.

[10] C.E. Daza, S. Moreno, R. Molina, Co-precipitated Ni-Mg-Al catalysts containing Ce for CO_2 reforming of methane, Int. J. Hydrogen Energ., 36 (2011) 3886-3894.

[11] A.I. Tsyganok, T. Tsunoda, S. Hamakawa, K. Suzuki, K. Takehira, T. Hayakawa, Dry reforming of methane over catalysts derived from nickel-containing Mg-Al layered double hydroxides, J. Catal., 213 (2003) 191-203.

[12] A.R. Gonzalez, Y.J.O. Asencios, E.M. Assaf, J.M. Assaf, Dry reforming of methane on Ni-Mg-Al nano-spheroid oxide catalysts prepared by the sol-gel method from hydrotalcite-like precursors, Appl. Surf. Sci., 280 (2013) 876-887.

[13] O.W. Perez-Lopez, A. Senger, N.R. Marcilio, M.A. Lansarin, Effect of composition and thermal pretreatment on properties of Ni-Mg-Al catalysts for CO_2 reforming of methane, Appl. Catal. A: Gen., 303 (2006) 234-244.

[14] Z.Y. Hou, T. Yashima, Meso-porous Ni/Mg/Al catalysts for methane reforming with CO_2, Appl. Catal. A : Gen., 261 (2004) 205-209.

[15] T. Shishido, M. Sukenobu, H. Morioka, R. Furukawa, H. Shirahase, K. Takehira, CO_2 reforming of CH_4 over Ni/Mg-Al oxide catalysts prepared by solid phase crystallization method from Mg-Al hydrotalcite-like precursors, Catal. Lett., 73 (2001) 21-26.

[16] A. Djaidja, S. Libs, A. Kiennemann, A. Barama, Characterization and activity in dry reforming of methane on NiMg/Al and Ni/MgO catalysts, Catal. Today, 113 (2006) 194-200.

[17] R. Debek, K. Zubek, M. Motak, P. Da Costa, T. Grzybek, Effect of nickel incorporation into hydrotalcite-based catalyst systems for dry reforming of methane, Res. Chem. Intermediates, in press, 10.1007/s11164-015-1973-x

[18] R. Debek, M. Radlik, M. Motak, M.E. Galvez, W. Turek, P. Da Costa, T. Grzybek, Ni-containing Ce-promoted hydrotalcite derived materials as catalysts for methane reforming with carbon dioxide at low temperature – On the effect of basicity, Catal. Today, in press, 10.1016/j.cattod.2015.03.017

[19] B. Koubaissy, A. Pietraszek, A.C. Roger, A. Kiennemann, CO_2 reforming of methane over Ce-Zr-Ni-Me mixed oxides, Catal. Today, 157 (2010) 436-439.

[20] M. Sharifi, M. Haghighi, F. Rahmani, S. Karimipour, Syngas production via dry reforming of CH_4 over Co- and Cu- promoted Ni/Al_2O_3-ZrO_2 nanocrystals synthesized via sequential impregnation and sol-gel methods, J. Narual Gas Sci. Eng., 21 (2014) 993-1004.

[21] J. Zhang, H. Wang, A.K. Dalai, Effects of metal content on activity and stability of Ni-Co bimetallic catalysts for CO_2 reforming of CH_4, Appl. Catal. A: Gen., 339 (2008) 121-129.

[22] F. Cavani, F. Trifiro, A. Vaccari, Hydrotalcite-Type Anionic Clays: Preparation, Properties and Applications, Catal. Today, 11 (1991) 173-301.

[23] O.D. Pavel, D. Tichit, I.C. Marcu, Acido-basic and catalytic properties of transition-metal containing Mg-Al hydrotalcites and their corresponding mixed oxides, Appl. Clay. Sci., 61 (2012) 52-58.

[24] J.I. Di Cosimo, V.K. Diez, M. Xu, E. Iglesia, C.R. Apesteguia, Structure and surface and catalytic properties of Mg-Al basic oxides , J. Catal., 178 (1998) 499-510.

[25] .I. Di Cosimo, C.R. Apesteguia, M.J.L. Gines, E. Iglesia, Structural requirements and reaction pathways in condensation reactions of alcohols on Mg_yAlO_x catalysts, J. Catal., 190 (2000) 261-275.

[26] L. Zhao, X.Y. Li, Z.P. Qu, Q.D. Zhao, S.M. Liu, X.J. Hu, The NiAl mixed oxides: The relation between basicity and SO 2 removal capacity, Sep. Purif. Technol., 80 (2011) 345-350.

Figures

Figure 1. DMR runs at 550°C, in the presence of the different catalysts: a) CH_4 conversion, b) CO_2 conversion, and c) ratio H_2/CO_2.

Figure 2. TEM images for a) HT-25Ni catalyst, at x 80,000, x 80,000 and x 400,000 augments, b) HTNi-Ce catalyst, at x 80,000, x 30,000 and x 400,000 augments, c) HTNi-Zr catalyst at x 80,000, x 300,000 and x 400,000 augments, and d) HTNi-CeZr catalyst, at x 80,000, x 120,000 and x 500,000 augments, all after 300 min DRM at 550°C.

Figure 3. Thermogravimetric oxidation of the carbon deposits in the spent HT-derived catalyst: Derivative of weight-loss as a function of temperature.

Figure 4. XRD patterns for a) the hydrotalcite materials before calcination, and b) the materials upon calcination, i.e. the different HT-derived catalysts.

Figure 5. a) Temperature programmed reduction (TPR) profiles and b) CO_2 temperature programmed desorption (TPD) for the Ce, Zr and CeZr promoted catalysts.

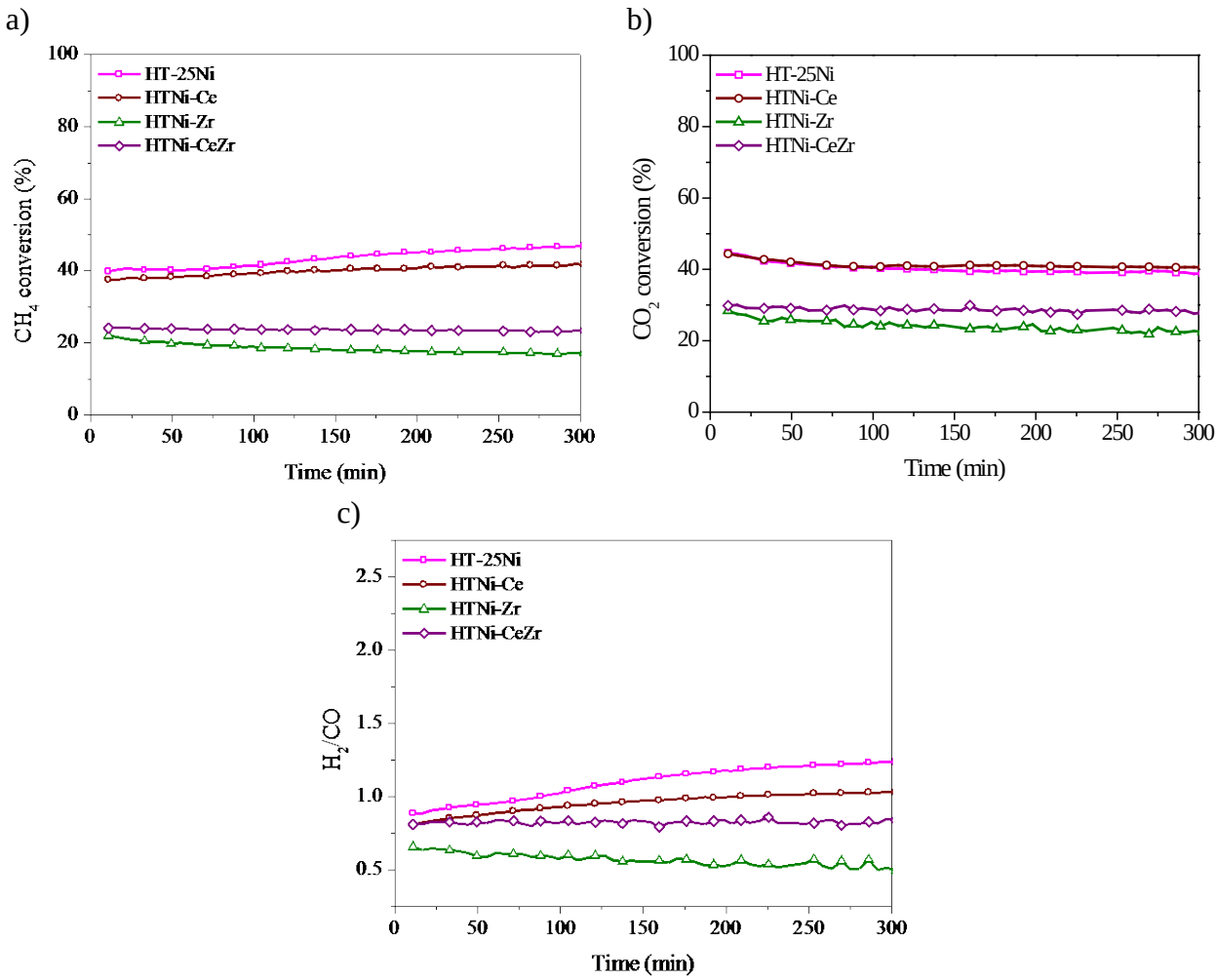

Figure 1. DRM runs at 550°C, in the presence of the different catalysts: a) CH_4 conversion, b) CO_2 conversion, and c) ratio H_2/CO_2.

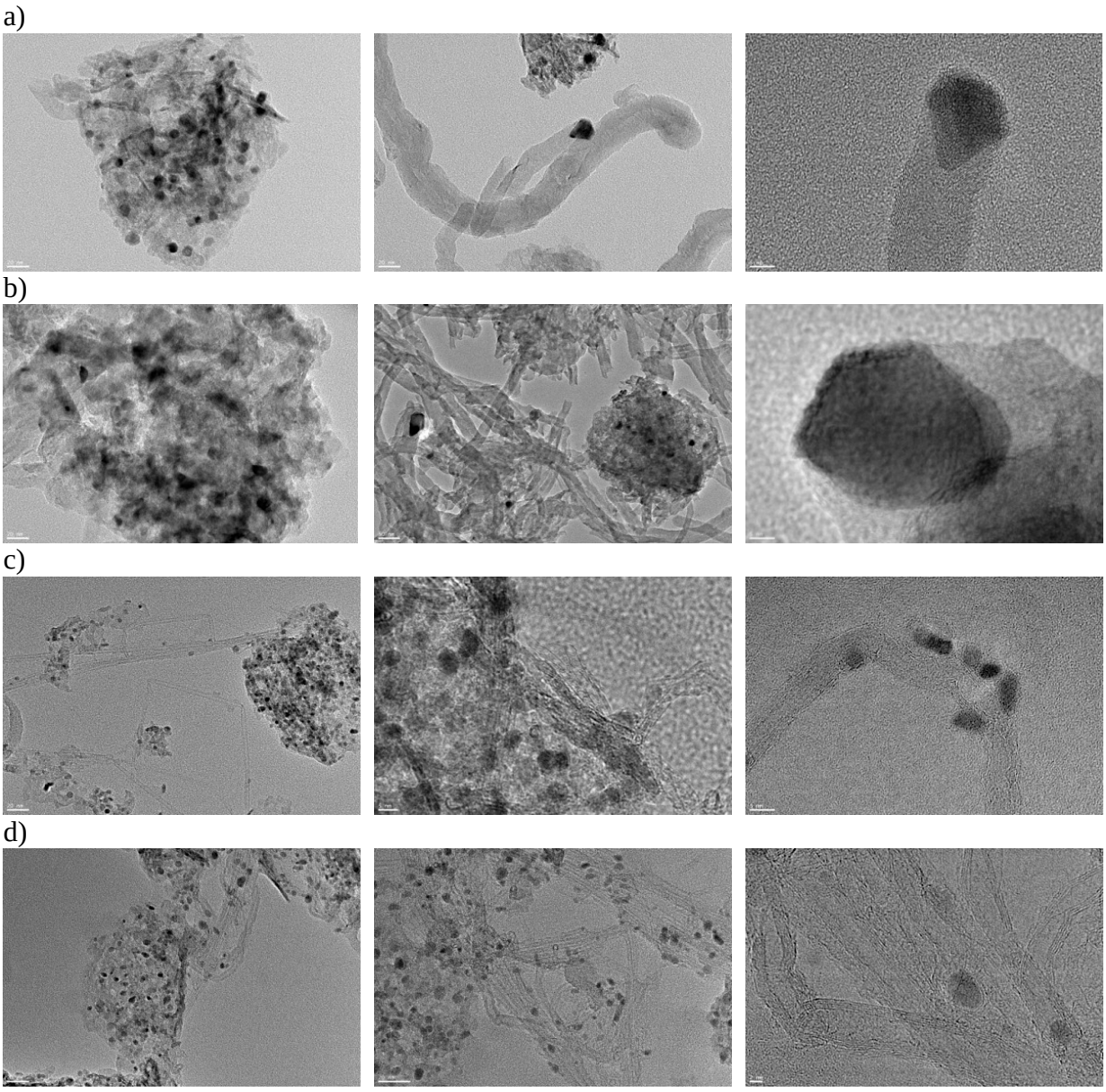

Figure 2. TEM images for a) HT-25Ni catalyst, at x 80,000, x 80,000 and x 400,000 augments, b) HTNi-Ce catalyst, at x 80,000, x 30,000 and x 400,000 augments, c) HTNi-Zr catalyst at x 80,000, x 300,000 and x 400,000 augments, and d) HTNi-CeZr catalyst, at x 80,000, x 120,000 and x 500,000 augments, all after 300 min DRM at 550°C.

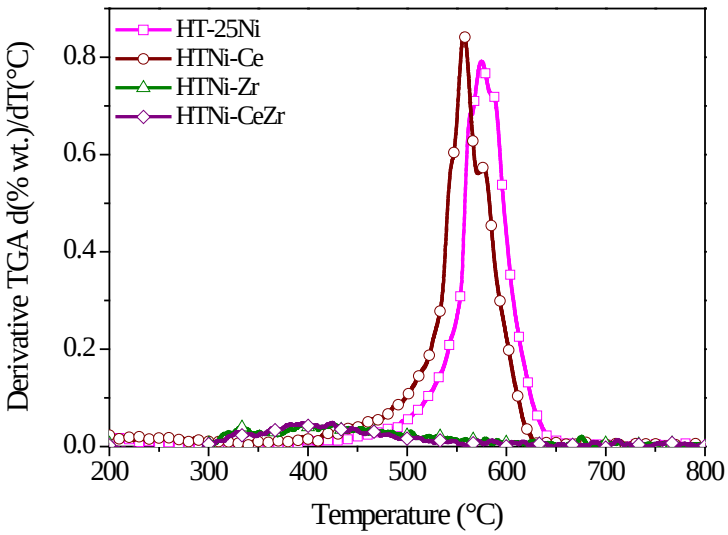

Figure 3. Thermogravimetric oxidation of the carbon deposits in the spent HT-derived catalyst: Derivative of weight-loss as a function of temperature.

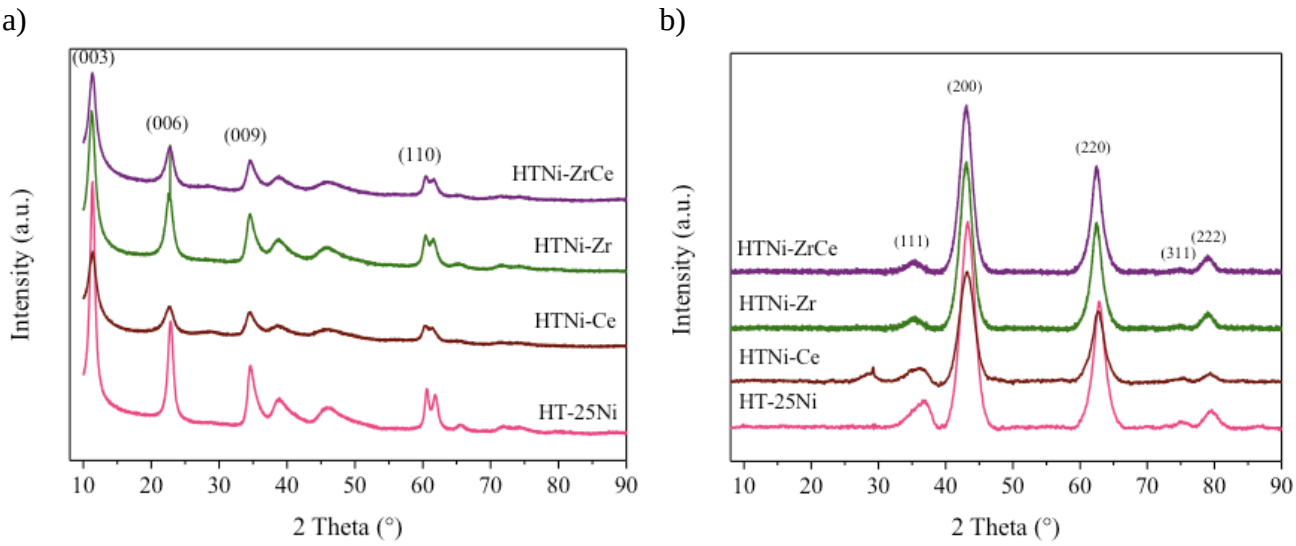

Figure 4. XRD patterns for a) the hydrotalcite materials before calcination, and b) the materials upon calcination, i.e. the different HT-derived catalysts.

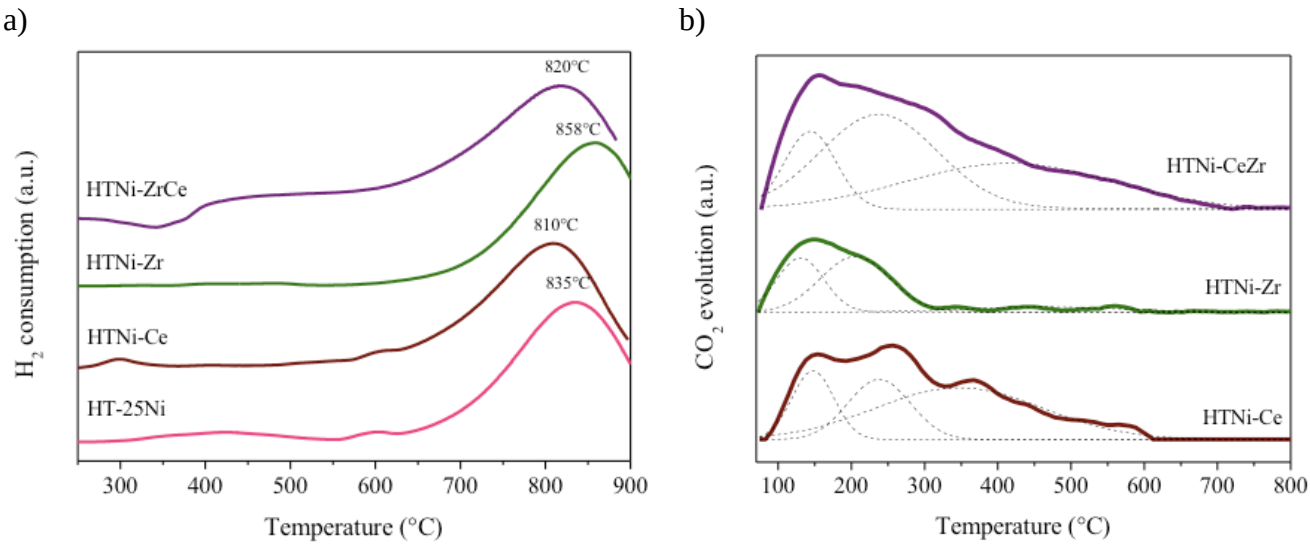

Figure 5. a) Temperature programmed reduction (TPR) profiles and b) CO_2 temperature programmed desorption (TPD) for the Ce, Zr and CeZr promoted catalysts.

Tables

Table 1. Composition and textural properties of the different HT-derived catalysts.

Catalyst	***Ni*** (wt.%)	***Mg*** (wt.%)	***Al*** (wt.%)	***Ce*** (wt.%)	***Zr*** (wt.%)	***Ni/Mg***	M^{2+}/M^{3+}	S_{BET} (m^2/g)	V_p (cm^3/g)	***Mean*** d_p (nm)
HT-25Ni	19.6	23.9	11.8	-	-	0.34	3.02	115	0.41	14
HTNi-Ce	17.9	21.5	10.8	3.7	-	0.34	2.96	102	0.33	13
HTNi-Zr	17.3	24	9.6	-	2.5	0.30	3.60	229	0.62	2.3
HTNi-CeZr	19.3	28.4	11.5	4.7	2.7	0.28	3.51	158	0.56	7.4